



UNIVERSITY OF LEEDS

This is a repository copy of *New Cross-Step Enabled Configurations for Humanoid Robot*.

White Rose Research Online URL for this paper:

<http://eprints.whiterose.ac.uk/148950/>

Version: Accepted Version

Proceedings Paper:

Xin, S, Zhou, C orcid.org/0000-0002-6677-0855 and Tsagarakis, N (2019) *New Cross-Step Enabled Configurations for Humanoid Robot*. In: *IEEE-RAS International Conference on Humanoid Robots. IEEE-RAS 18th International Conference on Humanoid Robots (Humanoids)*, 06-09 Nov 2018, Beijing, China. IEEE , pp. 1067-1072. ISBN 9781538672839

<https://doi.org/10.1109/HUMANOIDS.2018.8624982>

© 2018 IEEE. Personal use of this material is permitted. Permission from IEEE must be obtained for all other uses, in any current or future media, including reprinting/republishing this material for advertising or promotional purposes, creating new collective works, for resale or redistribution to servers or lists, or reuse of any copyrighted component of this work in other works.

Reuse

Items deposited in White Rose Research Online are protected by copyright, with all rights reserved unless indicated otherwise. They may be downloaded and/or printed for private study, or other acts as permitted by national copyright laws. The publisher or other rights holders may allow further reproduction and re-use of the full text version. This is indicated by the licence information on the White Rose Research Online record for the item.

Takedown

If you consider content in White Rose Research Online to be in breach of UK law, please notify us by emailing eprints@whiterose.ac.uk including the URL of the record and the reason for the withdrawal request.



eprints@whiterose.ac.uk
<https://eprints.whiterose.ac.uk/>

New Cross-step Enabled Configurations for Humanoid Robot

Songyan Xin, Chengxu Zhou, Nikos Tsagarakis

Abstract—This paper explores two new configurations for humanoid robot balancing and locomotion. Centroidal momentum manipulability analysis has been performed to study the features of the new configurations. Data collected from numerical simulation shows that they outperform the regular ones in terms of angular momentum manipulability. More importantly, the new configurations allow the humanoid robot to perform cross-step motions which is usually risky or mechanically impossible for most existing robots. On the other hand, cross-step also introduces non-convex feasible regions which makes it difficult to be incorporated into the existing step planner. A step region selector is thus proposed to transfer the step planning problem into a convex one by choosing a sub-convex region. To validate our ideas, cross-step is performed in simulation with a whole-body robot.

I. INTRODUCTION

For a humanoid robot, maintaining its balance is usually the first priority task to guarantee. Many criteria has been proposed to evaluate the stability of a humanoid system, and thus help to design a balance or locomotion controller. The most commonly used dynamic stability criteria requires that zero moment point (ZMP) [1], [2] or center of pressure (CoP) stays inside support polygon. Foot rotation indicator (FRI) [3] requires the foot has no rotation. Zero Rate of change of Angular Momentum (ZRAM) [4] guarantee rotationally stability. All these criteria summarize the robot stability on a reduced dimension geometry point and this compression unavoidably cause the loss of information. For example, two different stable configurations could ended up with the same ZMP (or CoP).

Most model-based balancing or locomotion planner use a simplified model to represent the essence of multi-rigid-body dynamics. These planner often generate references for Center of Mass (CoM) and end-effectors for the humanoid robot to track. The ability to track those references becomes extremely important for system controllability and thus stability. Manipulability of end-effector is a well-studied topic [5]–[7]. Similarly, this manipulability concept has been extended to ZMP point [8] and CoM point [9] [10] [11] [12]. Together with linear momentum, the angular momentum is also included in the centroidal momentum manipulability concept [13].

In this paper, the relationship between body postures and centroidal momentum manipulability has been studied. Two new configurations for the humanoid robot have been proposed as shown in Fig. 1. Cross-step which is enabled by

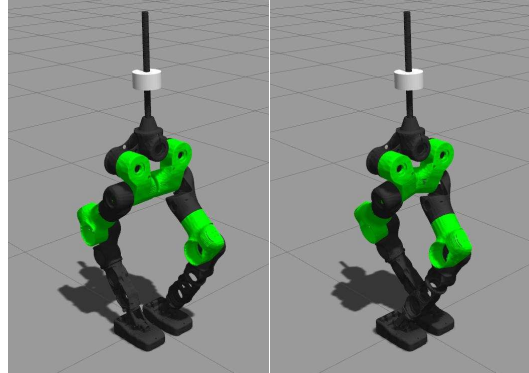


Fig. 1. Two new configurations for humanoid robot which enables it to perform cross-step. The left one is the result of bending the right knee of the robot backward. The right one could be achieved from the left one by crossing legs.

these configurations is then explored. Walking simulations are performed at the end to validate these configurations.

II. CENTROIDAL MOMENTUM MANIPULABILITY

The Centroidal Momentum Matrix (CMM) relates the robot’s generalized velocities to its centroidal momentum [13]:

$$\mathbf{h} = \mathbf{A}(\mathbf{q})\dot{\mathbf{q}} \quad (1)$$

where $\mathbf{A} \in \mathbb{R}^{6 \times (6+n)}$ is the CMM, $\mathbf{h} \in \mathbb{R}^{6 \times 1}$ is the centroidal momentum which consists the linear part $\mathbf{l} \in \mathbb{R}^{3 \times 1}$ and angular part $\mathbf{k} \in \mathbb{R}^{3 \times 1}$, $\dot{\mathbf{q}} \in \mathbb{R}^{(6+n) \times 1}$ is the generalized joint velocity which consists of the floating-base velocity $\dot{\mathbf{q}}_b = [\mathbf{v}_b, \boldsymbol{\omega}_b] \in \mathbb{R}^{6 \times 1}$ and actuated joint velocity $\dot{\mathbf{q}}_a \in \mathbb{R}^{n \times 1}$.

Centroidal momentum manipulability and corresponding ellipsoid are also proposed in [13]. Due to the scale disparities between the linear and angular part of the system momentum, it is preferred to construct two ellipsoids separately. More specifically, equation (1) can be expanded as:

$$\begin{bmatrix} \mathbf{l} \\ \mathbf{k} \end{bmatrix} = \begin{bmatrix} \mathbf{A}_l \\ \mathbf{A}_k \end{bmatrix} \dot{\mathbf{q}} = \begin{bmatrix} \mathbf{A}_{lb} & \mathbf{A}_{la} \\ \mathbf{A}_{kb} & \mathbf{A}_{ka} \end{bmatrix} \begin{bmatrix} \dot{\mathbf{q}}_b \\ \dot{\mathbf{q}}_a \end{bmatrix} \quad (2)$$

where \mathbf{l} , \mathbf{k} denote centroidal linear and angular momentum, so $\mathbf{A}_l \in \mathbb{R}^{3 \times (6+n)}$ and $\mathbf{A}_k \in \mathbb{R}^{3 \times (6+n)}$ are corresponding linear and angular momentum matrix. The subscript b and a indicate the base related part and configuration related part of corresponding momentum matrix. More specifically, $\mathbf{A}_{lb} \in \mathbb{R}^{3 \times 6}$ maps floating base velocity to system linear momentum and $\mathbf{A}_{la} \in \mathbb{R}^{3 \times n}$ maps the actuated joint velocity part.

Given the matrix \mathbf{A}_l , the linear momentum manipulability can be calculated as:

$$\omega_l = \sqrt{\det(\mathbf{A}_l \mathbf{A}_l^T)} \quad (3)$$

where $\det(*)$ denotes the determinant operation. The index ω_l measures the ability of transferring generalized joint velocity to system linear momentum of the humanoid robot at current configuration \mathbf{q} . This index is just a scaler indicator, more information can be visualized by constructing a ellipsoid from the matrix \mathbf{A}_l with Singular Value Decomposition (SVD),

$$\mathbf{A}_l = \mathbf{U} \mathbf{\Sigma} \mathbf{V}^T \quad (4)$$

where

$$\mathbf{U} = [\mathbf{u}_x \quad \mathbf{u}_y \quad \mathbf{u}_z] \quad (5)$$

$$\mathbf{\Sigma} = \begin{bmatrix} \sigma_x & 0 & 0 & \dots \\ 0 & \sigma_y & 0 & \dots \\ 0 & 0 & \sigma_z & \dots \end{bmatrix} \quad (6)$$

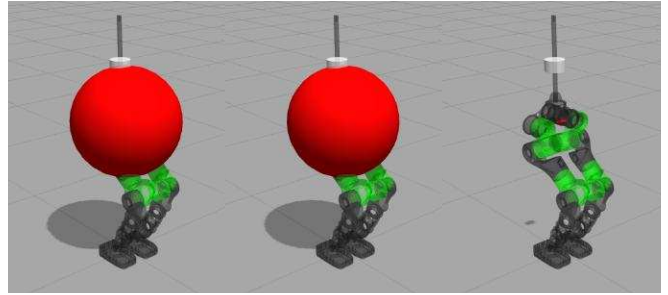
$$\mathbf{V}^T = [\mathbf{v}_1 \quad \mathbf{v}_2 \quad \dots \quad \mathbf{v}_m]^T \quad (7)$$

The principle axes of the ellipsoid are $\sigma_x \mathbf{u}_x$, $\sigma_y \mathbf{u}_y$ and $\sigma_z \mathbf{u}_z$. It is worth noting that the manipulability can be also calculated from singular values $\omega_l = \sqrt{\det(\mathbf{A}_l \mathbf{A}_l^T)} = \sqrt{\det(\mathbf{\Sigma} \mathbf{\Sigma}^T)} = \sigma_x \sigma_y \sigma_z$. The same process can be repeated for the angular momentum matrix \mathbf{A}_k and sub-matrices in Equation (2).

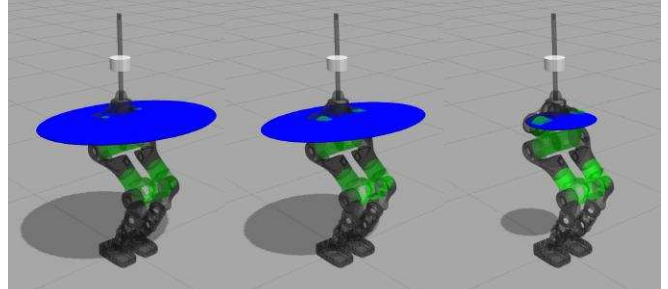
A. Manipulability Contribution

As stated in the previous section, the system momentum is contributed from floating base velocity $\dot{\mathbf{q}}_b$ and actuated joint velocity $\dot{\mathbf{q}}_a$. The previous part can be interpreted as base related contribution and the later part can be treated as configuration related contribution. In general, they contribute differently to system momentum. We are going to explore this in simulation with the lower body of our humanoid robot CogIMon.

The lower body of CogIMon has 12 actuated DoF (6 for each leg: 3 hip joints, 1 knee joint and 2 ankle joints). A fake mass link has been fixed on top of the pelvis link to represent the upper body. In simulation, the robot has been command to a given posture (CoM height equals to $0.8m$). Manipulability corresponding to sub-matrices in Equation (2) have been computed and listed in Table I. According to the data in the table, the contribution from floating base velocity $\dot{\mathbf{q}}_b$ dominant the linear part ($\omega_{l_a} : \omega_{l_b} = 1:3375$). However this is not the case for angular momentum, actuated joint velocity $\dot{\mathbf{q}}_a$ contributed a comparable part ($\omega_{k_a} : \omega_{k_b} = 1:6$) of angular momentum for the system. It is more straightforward to compare the contribution by observing the different manipulability ellipsoids shown in Fig. 2. All the results indicate that the actuated joint velocity $\dot{\mathbf{q}}_a$ has very limited contribution to the system linear momentum (or CoM velocity) but has a considerable amount of influence on the angular momentum. As a result, this paper will focus on studying how robot configuration contributes to the angular momentum of the system.



(a) Linear momentum ellipsoids generated from \mathbf{A}_l , \mathbf{A}_{l_b} and \mathbf{A}_{l_a}



(b) Angular momentum ellipsoids generated from \mathbf{A}_k , \mathbf{A}_{k_b} and \mathbf{A}_{k_a}

Fig. 2. Momentum manipulability ellipsoids. For better visualization, a scale factor 10^{-2} has been applied to those linear momentum ellipsoids. Because of the scale disparities between linear and angular momentum, a different scale factors 10^{-1} have been applied to angular momentum ellipsoids. Linear momentum ellipsoids have been plotted in red color and angular momentum ellipsoids in blue for differentiation.

B. Angular Momentum Manipulability of Different Configurations

In this part, four different configurations as shown in Fig. 3 are going to be examined. The *forward/forward* configuration is just like human with two knees bending forward. It is possible for a robot to bend its knees backward with proper mechanical design and which results in the *backward/backward* configuration. One analogy is the *elbow-up* and *elbow-down* configurations for a manipulator. A mix of the previous two leads to the *forward/backward* configuration. It can be further extended to a *twist* configuration by crossing step the left foot to the right side of the right foot.

To evaluate the angular momentum manipulability of these four configurations, the feet of the robot are initiated at the same location with respect to the ground (left foot and right foot is swapped in *twist* configuration) and the CoM is regulated to the same position (x and y take the position of the center of the feet, $z = 0.8m$). The configuration related angular momentum ellipsoids are plotted in the Fig. 4 and corresponding manipulability indexes are calculated and listed in Table II.

TABLE I
MANIPULABILITY CONTRIBUTION

Manipulability	ω	ω_b	ω_a	$\omega_a : \omega_b$
Linear momentum	209575.85	207226.92	61.40	1:3375
Angular momentum	66.03	42.73	6.63	1:6

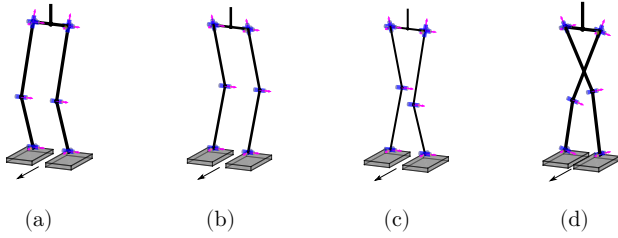


Fig. 3. Four configurations for humanoid robot (forward moving direction indicated by the arrows on the ground): (a) *forward/forward*; (b) *backward/backward*; (c) *forward/backward*; (d) *twist*. Here, *forward* and *backward* means knee configuration.

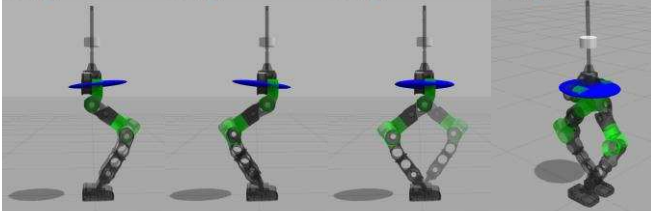


Fig. 4. Configuration related angular momentum ellipsoids of four different configurations from left to right: *forward/forward*, *backward/backward*, *forward/backward* and *twist*.

From Table II it can be seen that the configuration *forward/forward* and *backward/backward* have similar manipulability. However, these two configurations show different directional features (the first two plots in Fig. 4). Considering the principle axes of the ellipsoid as the optimum direction to generate angular momentum, the two configurations have different optimum directions. Both *forward/backward* and *twist* configurations give better manipulability than single sided configuration like *forward/forward* and *backward/backward*. Among all the configurations, *forward/backward* gives the best angular momentum manipulability.

C. Lift-up Motion

In the previous section, we concluded that the *forward/backward* configuration gives the best angular momentum manipulability. However the result only valid for the specific posture for which the corresponding CoM height is $0.8m$. In this section, the robot will be controlled to accomplish a lift up motion, the CoM will be commanded to move from its initial height $0.7m$ to $0.88m$. Configuration related angular momentum manipulability ω_{ka} will be recorded through out the process. Results for all four

TABLE II
ANGULAR MOMENTUM MANIPULABILITY OF DIFFERENT CONFIGURATIONS

Manipulability	<i>f/f</i>	<i>b/b</i>	<i>f/b</i>	<i>twist</i>
ω_k	66.03	66.04	90.78	74.54
ω_{kb}	42.73	43.13	54.42	42.15
ω_{ka}	6.63	6.59	10.37	9.36

Note: $f \rightarrow$ *forward*, $b \rightarrow$ *backward*

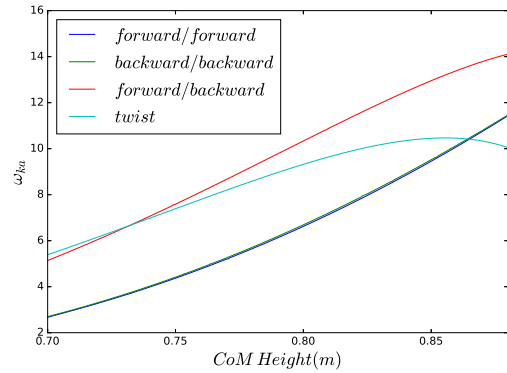


Fig. 5. Configuration related angular momentum manipulability through out the lift-up motion for different configurations.

configurations are plotted in the Fig. 5. It is obvious that the *forward/backward* is the best for this motion among the four configurations. The *twist* configuration shows good manipulability when the robot squat down, and decrease as the robot lift-up. The other two configurations have no difference for this motion. One might notes that the angular momentum manipulability indexes are generally increasing as the robot lift-up, this relationship is totally different comparing to the linear ones which in this case decrease. This can be interpreted as: the masses of the robot distributed further away from the CoM, so they have longer moment arm to influence the centroidal angular momentum.

III. CROSS-STEP

The proposed configurations *forward/backward* and *twist* give better angular momentum manipulability for a wide range of postures. They bring not only better manipulability to the robot, but also new motion possibility: cross-step.

Most existing disturbance rejection methods use model predictive control (MPC) to updates foot placement online [14] [15] [16] [17]. Since online iterative optimization involved in the MPC method, linear model is usually chosen as template model. Non-linear formulation which involve step timing optimization have been explored in several studys [18] [19] [20]. Considering the worst case scenario in which the robot has been heavily pushed towards the right during the right support phase, a two step strategy is necessary: put down the left foot as close as possible to the right foot within as short as possible duration, followed a large right side step. For human, a more natural reaction would be cross their legs to make a cross step directly. This action is however risky or mechanically impossible for most existing robots. The proposed configurations *forward/backward* or *twist* could be a solution to this problem. The cross-step action with *forward/backward* configured robot is shown in the Fig. 6. As can be seen from the figure, the robot switches from *forward/backward* configuration to *twist* configuration with one cross step. The switching can happen infinitely which means the robot can do multiple cross-steps continuously as plotted in Fig. 7.

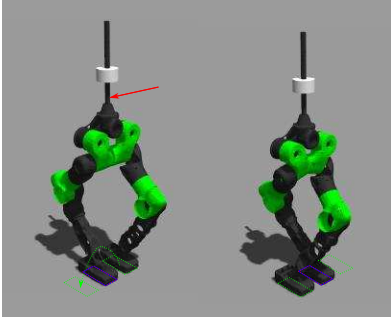


Fig. 6. Corss-step action. The red arrow indicates a push force from left to right acting on the robot at a certain moment, and this initiates the cross-step action: the left foot swing over the right foot and lands on the right side of it. Self-collision can be observed between the hip-pitch links, this is due to the fact that the mechanical design is finished before we come up with this cross-step idea. But it is fully possible to avoid this problem with proper new design.

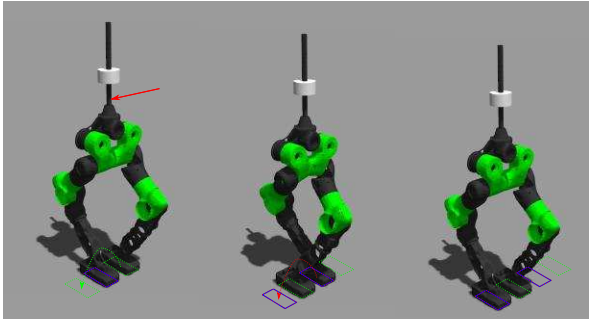


Fig. 7. Multiple corss-steps. Footprints has been labeled with squares, the green ones represent the left footprints and the red ones are for the right foot.

A. Foot step planning

With the possibility to do cross-step action, the feasible region for the swing foot is enlarged. For footstep planning, the feasible region \mathcal{F} of the swing foot is usually defined by:

$$\mathcal{F} \in \mathcal{D} \cap \mathcal{K} \cap \mathcal{C} \quad (8)$$

where \mathcal{D} is the design region, \mathcal{K} is the kinematic feasible region, \mathcal{C} is the collision-free region. For the two cases illustrated in Fig. 8, they have different design region \mathcal{D} :

$$\mathcal{D}_{f/f} = \{(x, y) \in \mathbb{R}^2 \mid y > w\} \quad (9)$$

$$\mathcal{D}_{f/b} = \{(x, y) \in Q_I \cup Q_{II} \cup Q_{IV}\} \quad (10)$$

where w is the width of the footprint, f/f and f/b stands for *forward/forward* and *forward/backward*. The later configuration increased the design region with considerable amount.

B. Walking Controller

A two-level controller has been used to generate the whole-body motion for the robot. The foot-step planner uses linear inverted pendulum model (LIPM) as template model [21]. The model is composed of a point mass and a massless telescopic leg. Therefore, the planner based on this model provide no information about the configuration of the robot. It only generates Cartesian space references such as CoM

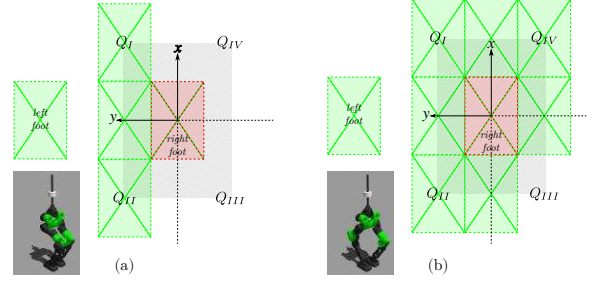


Fig. 8. Design region for left swing foot while the robot takes different configuration: (a) *forward/forward*, (b) *forward/backward*. Assuming in right single support phase, a fixed frame is attached to the center of right stance foot and it is plotted in red. The swing left foot is in green and several possible landing prints have been plotted for reference. Grey strip label out unfeasible regions due to self-collisions between two feet.

and feet trajectories. The planner is formulated as a liner model predictive control problem which optimizes future steps for the robot. The formulation is similar to those in paper [16] [17] in spirit, but the details differs. In those two papers, several future foot placements are always generated at touchdown moment and used as references for later online footstep optimization. By minimizing the error between planning footsteps and the desired references, the results will converge. However for our case as shown in (b) of Fig. 8, the stance foot makes the feasible region non-convex, in this case, we have to select a convex sub-region to make problem convex and solvable. In this paper, this is accomplished in a heuristic approach: a simple design region selector will take the commanded robot walking velocity and disturbances as inputs and select proper region to generate reference foot placements. The whole-body controller is formulated as a quadratic optimization problem. Given desired CoM and feet trajectories, the controller will find out the joint-torques to full fill them and at the same time with respect to constraints, such as dynamic feasibility, friction cone, torque limits. The robot is simulated in Gazebo, each joint of the robot is purely torque controlled. Odometry data and joint states (positions and velocities) has been sent back from gazebo as feedback for next step planning and control. The whole-body controller is running at 1000 Hz and the planner is running at a lower frequency.

Walking motion in different direction have been simulated. Shown in Fig. 9, the one above is cross-stepping and the one below is walking forward. Only a new velocity command is needed to change the walking direction of the robot. After receiving the command, the planner will generate reference foot placements based on it. Without the presence of any disturbances, a large velocity in y direction would trigger the cross-step motion and a small one would results in small side step without crossing legs. A strong side push on the robot could also trigger the cross-step in the same direction. These two thresholds are both set in the design region selector as mentioned before. One thing worth noting is that the robot does not have to switch back to *forward/backward* to be able to walk forward. That is to say, the robot can perform

walking forward motion in *twist* configuration as shown in Fig. 10. This guarantees the robot could change walking direction at any stage of cross-step.

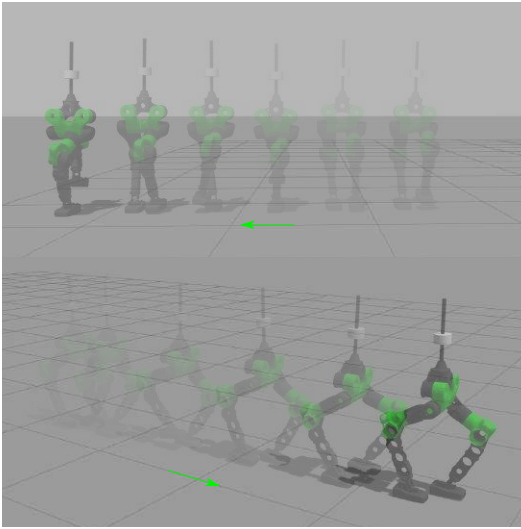


Fig. 9. Robot walking in different direction. Green arrows denote the walking direction.

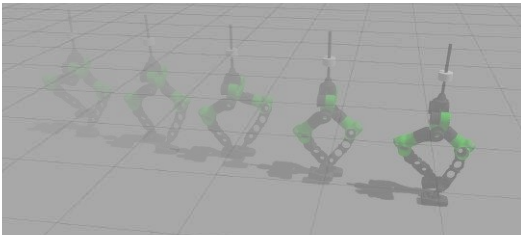


Fig. 10. Robot walking forward in *twist* configuration.

IV. CONCLUSION

In this paper, we propose two new configurations for humanoid balancing and walking. We have compared them with other regular configurations in terms of centroidal momentum manipulability. They indeed provide better angular momentum manipulability. One major benefit of the proposed configurations is the new cross-step motion. This is a very useful skill in push recovery but long being ignored due to hardware limitations. With cross-step, the robot is more robust in lateral direction. But this skill also brings new problems to the step planner. With non-convex feasible region, traditional convex optimization can not directly be applied on it. We came up with a new design region selector on top of the step planner to overcome this problem. Based on the commanded velocity and disturbance detection, the selector can make directional step decision before generating reference foot step placements. Whole-body robot walking simulation has been performed to verify the proposed cross-step idea.

ACKNOWLEDGMENT

This work is supported by European Community's Horizon 2020 robotics program CogIMon (ICT-23-2014, 644727).

REFERENCES

- [1] M. Vukobratovic, A. Frank, and D. Juricic, "On the stability of biped locomotion," *IEEE Transactions on Biomedical Engineering*, no. 1, pp. 25–36, 1970.
- [2] M. Vukobratović and B. Borovac, "Zero-moment point thirty five years of its life," *International Journal of Humanoid Robotics*, vol. 1, no. 01, pp. 157–173, 2004.
- [3] A. Goswami, "Foot rotation indicator (fri) point: A new gait planning tool to evaluate postural stability of biped robots," in *Robotics and Automation, 1999. Proceedings. 1999 IEEE International Conference on*, vol. 1. IEEE, 1999, pp. 47–52.
- [4] A. Goswami and V. Kallem, "Rate of change of angular momentum and balance maintenance of biped robots," in *Robotics and Automation, 2004. Proceedings. ICRA'04. 2004 IEEE International Conference on*, vol. 4. IEEE, 2004, pp. 3785–3790.
- [5] T. Yoshikawa, "Manipulability of robotic mechanisms," *The international journal of Robotics Research*, vol. 4, no. 2, pp. 3–9, 1985.
- [6] T. Yoshikawa, "Dynamic manipulability of robot manipulators," *Transactions of the Society of Instrument and Control Engineers*, vol. 21, no. 9, pp. 970–975, 1985.
- [7] A. Bowling and O. Khatib, "The dynamic capability equations: a new tool for analyzing robotic manipulator performance," *IEEE transactions on robotics*, vol. 21, no. 1, pp. 115–123, 2005.
- [8] N. Naksuk and C. G. Lee, "Zero moment point manipulability ellipsoid," in *Robotics and Automation, 2006. ICRA 2006. Proceedings 2006 IEEE International Conference on*. IEEE, 2006, pp. 1970–1975.
- [9] N. Naksuk and C. G. Lee, "Utilization of movement prioritization for whole-body humanoid robot trajectory generation," in *Robotics and Automation, 2005. ICRA 2005. Proceedings of the 2005 IEEE International Conference on*. IEEE, 2005, pp. 1079–1084.
- [10] S. Cotton, P. Fraisse, and A. P. Murray, "On the manipulability of the center of mass of humanoid robots: Application to design," in *ASME 2010 International Design Engineering Technical Conferences and Computers and Information in Engineering Conference*. American Society of Mechanical Engineers, 2010, pp. 1259–1267.
- [11] Y. Gu, C. G. Lee, and B. Yao, "Feasible center of mass dynamic manipulability of humanoid robots," in *Robotics and Automation (ICRA), 2015 IEEE International Conference on*. IEEE, 2015, pp. 5082–5087.
- [12] M. Azad, J. Babič, and M. Mistry, "Dynamic manipulability of the center of mass: A tool to study, analyse and measure physical ability of robots," in *Robotics and Automation (ICRA), 2017 IEEE International Conference on*. IEEE, 2017, pp. 3484–3490.
- [13] D. E. Orin and A. Goswami, "Centroidal momentum matrix of a humanoid robot: Structure and properties," *dynamics*, vol. 4, p. 6, 2008.
- [14] A. Herdt, H. Diedam, P.-B. Wieber, D. Dimitrov, K. Mombaur, and M. Diehl, "Online walking motion generation with automatic footstep placement," *Advanced Robotics*, pp. 719–737, 2010.
- [15] J. Urata, K. Nshiwaki, Y. Nakanishi, K. Okada, S. Kagami, and M. Inaba, "Online decision of foot placement using singular lq preview regulation," in *Humanoid Robots (Humanoids), 2011 11th IEEE-RAS International Conference on*. IEEE, 2011, pp. 13–18.
- [16] S. Faraji, S. Pouya, C. G. Atkeson, and A. J. Ijspeert, "Versatile and robust 3d walking with a simulated humanoid robot (atlas): A model predictive control approach," in *Robotics and Automation (ICRA), 2014 IEEE International Conference on*. IEEE, 2014, pp. 1943–1950.
- [17] S. Feng, X. Xinjilefu, C. G. Atkeson, and J. Kim, "Robust dynamic walking using online foot step optimization," in *Intelligent Robots and Systems (IROS), 2016 IEEE/RSJ International Conference on*. IEEE, 2016, pp. 5373–5378.
- [18] P. Kryczka, P. Kormushev, N. G. Tsagarakis, and D. G. Caldwell, "Online regeneration of bipedal walking gait pattern optimizing footstep placement and timing," in *Intelligent Robots and Systems (IROS), 2015 IEEE/RSJ International Conference on*. IEEE, 2015, pp. 3352–3357.

- [19] M. Khadiv, A. Herzog, S. A. A. Moosavian, and L. Righetti, "Step timing adjustment: A step toward generating robust gaits," in *Humanoid Robots (Humanoids), 2016 IEEE-RAS 16th International Conference on*. IEEE, 2016, pp. 35–42.
- [20] W. Hu, I. Chatz Nikolaidis, K. Yuan, and Z. Li, "Comparison study of nonlinear optimization of step durations and foot placement for dynamic walking," *arXiv preprint arXiv:1805.02155*, 2018.
- [21] S. Kajita, F. Kanehiro, K. Kaneko, K. Fujiwara, K. Harada, K. Yokoi, and H. Hirukawa, "Biped walking pattern generation by using preview control of zero-moment point," in *International Conference on Robotics and Automation*, 2003, pp. 1620–1626.